Draft version November 12, 2021
Typeset using LaTeX **twocolumn** style in AASTeX631

TIC 5724661: A Long-Period Binary with a Pulsating sdB Star and δ Scuti Variable

Rahul Jayaraman [1], Saul A. Rappaport,[1] Lorne Nelson [2], Donald W. Kurtz [3,4], George Dufresne,[2] Gerald Handler,[5] Abdel Senhadji [2,6], David W. Latham [7], George Zhou,[7] Allyson Bieryla [7] and George R. Ricker[1]

[1] *MIT Department of Physics and MIT Kavli Institute for Astrophysics and Space Research, Cambridge, MA 02139, USA*
[2] *Department of Physics and Astronomy, Bishop's University, 2600 College St., Sherbrooke, QC J1M 1Z7, Canada*
[3] *Centre for Space Research, Physics Department, North West University, Mahikeng 2745, South Africa*
[4] *Jeremiah Horrocks Institute, University of Central Lancashire, Preston PR1 2HE, United Kingdom*
[5] *Nicolaus Copernicus Astronomical Center of the Polish Academy of Sciences, Bartycka 18, 00-716 Warsaw, Poland*
[6] *Department of Physics, University of New South Wales Canberra, Northcott Dr., Campbell, ACT 2600, Australia*
[7] *Center for Astrophysics — Harvard & Smithsonian, 60 Garden St., Cambridge, MA 02138, USA*

(Received November 12, 2021; Revised November 12, 2021; Accepted November 12, 2021)

ABSTRACT

Using the novel *TESS* 20-sec cadence data, we have discovered an unusual combination of pulsating stars in what we infer to be a binary system. The primary is a standard δ Scuti star with pulsations over the range 32-41 d^{-1}; this is in an inferred wide orbit with a hot subdwarf B (sdB) secondary, which itself has a large-amplitude p-mode pulsation at 524 d^{-1}. We establish an constraints on the period of the putative binary by using radial velocity measurements of the δ Scuti star and show that any sdB-mass companion star must have an orbital period greater than ~ 35 d. Our identification of this sdB binary serves as an important addition to the relatively small amount of sdB binaries known to have a period longer than a few days. We show that such a binary can be formed through stable, nonconservative mass transfer, without undergoing a common envelope phase.

1. INTRODUCTION

1.1. *Observational properties of hot subdwarfs*

Hot subdwarf stars are core helium-burning stars with a thin hydrogen envelope that exhibit significant chemical peculiarities. Such stars represent late stages in stellar evolution and are believed to be the stripped cores of red giants. They typically lie on the blue end of the Extreme Horizontal Branch (EHB) of the Hertzsprung-Russell Diagram (HRD; see, e.g., Heber 1986; Saffer et al. 1994; Heber 2016). These stars have surface temperatures ranging from $20,000 \lesssim T_{\rm eff} \lesssim 60,000$ K, with $5 \lesssim \log g \lesssim 6.5$. While their spectra appear similar to main-sequence (MS) stars of the same spectral type, they tend to be much smaller and greatly underluminous for their $T_{\rm eff}$, but are rather overluminous for their mass – with masses close to 0.45 $M_\odot$. Of this, 0.01 $M_\odot$ is contained within a thin hydrogen shell at the surface.

Corresponding author: Rahul Jayaraman
rjayaram@mit.edu

There are several classes of subdwarf stars; this fact is supported by the work of (Senhadji 2019), who calculated a grid of $\sim$3000 subdwarf progenitor binary models. It was found that subdwarf B (sdB) stars tend to have lower values of $T_{\rm eff}$ and $\log g$ when compared to subdwarf O (sdO) stars. The overlying hydrogen layer appears to become more depleted as these stars evolve from sdBs into sdOs. A more recent class, the sdA stars (identified by Kepler et al. 2016), have spectra consistent with $5.5 \lesssim \log g \lesssim 6.5$, and $T_{\rm eff} \lesssim 20{,}000$ K. However, there has not been a definitive explanation as to the true nature of these objects. This paper will primarily focus on sdB stars, and occasionally mention sdO stars, when relevant in an evolutionary context.

1.2. *Pulsating subdwarfs*

The first pulsating sdB (sdBV) star, EC 14026-2647, was discovered by Kilkenny et al. (1997), who found a pulsation with a period of 144 s. Since then, over 100 such pulsating stars have been discovered (Holdsworth et al. 2017). These stars fall into three categories – rapid ($\rm sdBV_r$) pulsators, with p mode oscillations on the order of a few minutes; slow ($\rm sdBV_s$) pulsators, with g mode

oscillations on the order of a few hours, and hybrid pulsators, which exhibit both p and g mode oscillations.

While the different classes of sdBV are fairly well-defined, the formation of these objects remains somewhat of a mystery. In brief, for sdB stars in short-period binaries, the most promising theory is that of common-envelope evolution, in which the sdBV progenitor overfills its Roche lobe and achieves a sufficiently high mass transfer rate onto its companion (Mengel et al. 1976). Such a high accretion rate precludes the companion star from accreting all of the deposited matter, leading to the formation of a common envelope (see, e.g., Kuiper 1941; for a description of common envelopes in the context of sdB evolution, see Han et al. 2002). The relatively high proportion of sdB stars observed in short-period binaries suggests that this evolutionary scenario is the most common (Han et al. 2003), but there exists an observational bias that favors the discovery of such systems. Theories for the formation of medium- and long-period sdB binaries center on the role of stable, (non)conservative mass transfer. A detailed discussion of the evolution of different types of binaries containing sdB stars can be found in Section 6.1, the references therein, and in the seminal papers of Han et al. (2002) and Han et al. (2003).

1.3. *TIC 5724661*

As part of its goal to enable precision asteroseismology, the Transiting Exoplanet Survey Satellite (*TESS*; Ricker et al. 2015) has been observing a subset of stars using a novel 20-second cadence since Sector 27, which occurred during July 2020. This mode can probe frequencies up to a Nyquist limit of 2160 d^{-1}, corresponding to periods as short as 40 s. *TESS* short-cadence observations are invaluable in the detection and characterization of new subdwarfs, especially pulsators (see Section 6 of Lynas-Gray 2021, and references therein).

TIC 5724661 was chosen to be observed at 20 s cadence because it was a known A star in the instability strip on the HRD. Observations of this star and our subsequent analyses revealed two sets of pulsational frequencies – one in the typical δ Scuti frequency range and two other, unexpected, peaks at 524 d^{-1} and 580 d^{-1}. These two are in the characteristic pulsational frequency range of hot compact stars, like white dwarfs and sdBV$_\mathrm{r}$ stars.

In this paper, we first analyze the frequencies of the δ Scuti pulsations and discuss the modes they represent. Then, we show that the spectrum of TIC 5724661 does not exhibit the chemical abnormalities of a roAp star. Moreover, no significant variations in radial velocity are found over a series of unequally-spaced observations, suggesting a long-period ($\gtrsim$ 70 d) orbit. We next discuss the strong evidence for a hot compact companion suggested by the excess ultraviolet (UV) flux in the Spectral Energy Distribution (SED). We then explore possible formation pathways for such a system and contextualize our discovery of a novel system. Note, we will hereafter refer to the A-star component of the binary as the "secondary", and the sdB component as the "primary", for reasons regarding the evolution of the binary that will be more thoroughly explained in Section 6.

Table 1. Properties of TIC 5724661

Parameter	Value
RA (J2015.5) (h m s)	23:11:07.84
Dec (J2015.5) (° ′ ″)	-17:13:19.424
T^a	11.204 ± 0.007
G^b	11.286 ± 0.001
$G_{\mathrm{BP}}{}^b$	11.353 ± 0.001
$G_{\mathrm{RP}}{}^b$	11.154 ± 0.001
B^a	11.431 ± 0.129
V^a	11.231 ± 0.010
J^c	10.998 ± 0.020
H^c	10.962 ± 0.024
K^c	10.919 ± 0.023
$\mathrm{W1}^d$	10.889 ± 0.023
$\mathrm{W2}^d$	10.917 ± 0.020
$\mathrm{W3}^d$	10.851 ± 0.162
$\mathrm{W4}^d$	> 8.607
R $(\mathrm{R}_\odot)^e$	$1.32^{+0.09}_{-0.11}$
L $(\mathrm{L}_\odot)^e$	5.737 ± 0.8
Distance $(\mathrm{pc})^b$	611 ± 15
μ_α $(\mathrm{mas\ yr}^{-1})^b$	-4.5197 ± 0.0375
μ_δ $(\mathrm{mas\ yr}^{-1})^b$	$+4.941 \pm 0.0304$

Notes. (a)exofop.ipac.caltech.edu/tess/index.php. (b) *Gaia* eDR3 (Gaia Collaboration et al. 2016a; Gaia Collaboration et al. 2016b; Gaia Collaboration et al. 2021). (c) 2MASS catalog (Skrutskie et al. 2006). (d) WISE point source catalog (Cutri & et al. 2014). (e) This work; see Table 4 for details regarding the radius estimate, as well as Table 2 for RV data.

2. OBSERVATIONAL DATA

2.1. *TESS Observations of TIC 5724661*

TIC 5724661 was observed by *TESS* in Sector 29 (from 2020 August 26 to September 21) and Sector 42 (from 2021 August 20 to September 16) in both 2 min and 20 s cadence. The data are available in both SAP (simple aperture photometry) and PDCSAP (presearch data conditioning SAP) forms. Data processing was done using the SPOC pipeline at NASA Ames (Jenkins 2015). We used the PDCSAP data from only Sector 29 for our analysis after converting the given flux intensity to mag-

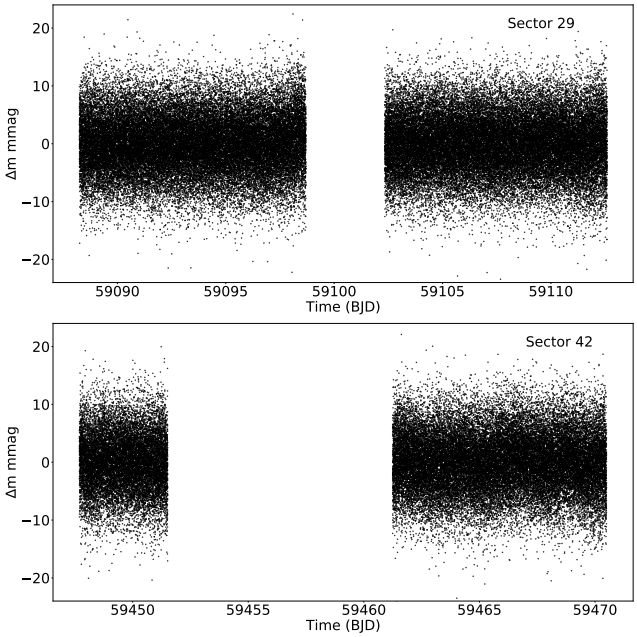

Figure 1. The light curve of TIC 5724661 obtained in 20 s cadence in *TESS* Sectors 29 and 42 after processing with the SPOC pipeline (Jenkins 2015). The pulsations are too rapid and too low in amplitude to discern visually in this compressed figure. Its purposes are (i) to show the two gaps in the data, which affect the spectral window, and (ii) to show the noise level in the 20-s data points. The ordinate scale is Barycentric Julian Date – 240 0000.0.

nitudes.[1] The data from Sector 29 span 24.33 d with a temporal center point of t_0 = BJD 2459100.41122, and comprise 88937 data points (after clipping by SPOC to remove outlier points, e.g., those arising from cosmic ray strikes on the detector).[2]

Figure 1 shows the SPOC-processed light curves with the data gaps between the two orbits making up each *TESS* sector. These arise from the lack of observations during data downlink, or saturation of the CCDs due to scattered light from the Earth and the Moon. Such data gaps affect the spectral window, necessitating either analysis with a Discrete Fourier Transform (DFT; see, e.g., Kurtz 1985) or appropriate corrections, such as re-binning the data into equally-spaced temporal bins.

2.2. *Spectroscopy*

We obtained spectroscopic observations of the target TIC 5724661 with the Tillinghast Reflector Echelle Spectrograph (TRES, Furesz 2008), on the 1.5-m reflector at the Fred Lawrence Whipple Observatory (FLWO) in Arizona, USA. TRES is a high-resolution fiber-fed echelle spectrograph, with a spectral resolving power of R = 44 000 over the wavelength region of 3900 – 9100 Å. A total of seven observations were obtained for TIC 5724661 during 2020 December, and between 2021 September and 2021 November, with peak signal-to-noise ratios per resolution element of ∼30 in the Mg b triplet wavelength region. The spectra were extracted and reduced as per Buchhave et al. (2010), with wavelength solutions derived from bracketing Th-Ar lamp exposures. The observing schedule was designed to be sensitive to a companion with an orbital period $P_{\rm orb} \lesssim 30$ d.

To derive the spectroscopic broadening profiles and radial velocities from each observation, we performed a least-squares deconvolution (LSD, Donati et al. 1997) of each spectrum against a synthetic non-rotating template; this provided both a value for the radial velocity, along with an uncertainty value. We also conducted a multi-order velocity analysis of the spectra, and derived another set of uncertainties for the radial velocity values. We observed that the multi-order uncertainties were around 50% greater than the LSD uncertainties. These values are presented in Table 2.

Visual examination of the broadening profiles for a set of lines from the sdB companion remained negative, but the line profiles did show night-to-night variability consistent with typical spectroscopic line variations exhibited by δ Scuti stars. The broadening profiles were fitted with a model kernel accounting for the rotational, macroturbulent, and instrumental broadening terms, as well as the velocity shift of the spectrum. The comparison to model spectra and further analyses (including the use of a rotating template) are described in Section 4.

Table 2. Radial Velocity Measurements of TIC 5724661 from the Tillinghast Reflector Echelle Spectrograph (TRES)

Observation Date (BJD-2400000)	Radial Velocity ($\rm km\,s^{-1}$)	LSD Error ($\rm km\,s^{-1}$)	Multi-Order Error ($\rm km\,s^{-1}$)
59190.6081	−39.85	± 0.17	± 1.08
59196.5855	−39.54	± 0.73	± 0.89
59199.5753	−41.06	± 0.80	± 0.92
59200.5938	−40.24	± 0.66	± 0.93
59202.5893	−41.05	± 0.69	± 1.18
59484.7757	−39.03	± 0.63	± 0.93
59487.7216	−38.98	± 0.38	± 0.97
59519.6938	−37.51	± 0.47	± 0.57

[1] The data from Sector 42 have a large data gap during the first orbit (see Figure 1) due to saturation of the CCDs arising from the moon being in the TESS field-of-view.

[2] TESS Sector 29 Data Release Notes: https://archive.stsci.edu/missions/tess/doc/tess_drn/tess_sector_29_drn43_v02.pdf

-39.85025 -39.5396 -41.06128 -40.24003 -41.04946 -39.0269 -38.98179 -37.5082

The set of seven measured radial velocities obtained with TRES is given in Table 2.

3. FREQUENCY ANALYSIS

The *TESS* data from both Sectors 29 and 42 were analyzed using a fast Discrete Fourier Transform (Kurtz 1985) to produce amplitude spectra. The top panel in Fig. 2 shows the amplitude spectrum out to about half the Nyquist frequency of 2160 d^{-1}, calculated using the Sector 29 data. A cluster of peaks in the δ Sct frequency range is seen between $26 - 46\,\mathrm{d}^{-1}$, and a single, high-frequency peak is clearly detected at $523.99\,\mathrm{d}^{-1}$ (6.065 mHz). These are shown at higher frequency resolution in the two middle panels, with appropriate labels indicating the sector whose data was input to the DFT.

We fitted the 13 δ Sct frequencies and the most prominent sdBV$_\mathrm{r}$ frequency to the Sector 29 data using a non-linear least-squares algorithm in order to (a) optimize the frequencies, amplitudes and phases, and (b) determine their uncertainties. Those best-fit parameters are provided in Table 3. The frequency range is narrow, and the number of excited modes is relatively small for a δ Sct star. The bottom panel of Figure 2 shows the amplitude spectrum of the residuals after a non-linear least-squares fit of the 14 aforementioned peaks was subtracted from the data. We believe that the highest-frequency peak, at $523.99\,\mathrm{d}^{-1}$ arises from a pulsation mode in an sdBV$_\mathrm{r}$ star, as discussed later.

A simple zeroth order relation for a pulsator (first derived using a toy model in Ritter 1879) that relates the pulsation period P and mean density $\bar{\rho}$ is:

$$P\sqrt{\frac{\bar{\rho}}{\bar{\rho}_\odot}} = Q, \tag{1}$$

where Q is a constant for a given pulsation mode, which is defined by this equation. This can be rewritten in terms of observables as follows:

$$\log Q = \log P + \frac{1}{2}\log g + \frac{1}{10}M_\mathrm{bol} + \log T_\mathrm{eff} - 6.454, \tag{2}$$

Here, P is in days and $\log g$ is in cgs units. As a first-order estimate, we use the *TESS* input catalog (TIC) values of $T_\mathrm{eff} = 8400\,\mathrm{K}$ and $\log g = 4.3$ (Stassun et al. 2019) and estimate $M_\mathrm{bol} = 1.6\,\mathrm{mag}$ from the *Gaia* parallax and V magnitude. Thus, we can calculate the Q-values for the δ Sct frequencies, which enables us to estimate the radial overtone for these frequencies' modes by comparing them with previously-calculated models, such as those in Table 1 of Stellingwerf (1979). Note that the putative sdB companion is significantly fainter in the *TESS* and *Gaia* passbands (i.e., in the optical – see Figure 4), so its contribution to the total absolute magnitude of the system can be neglected here.

For the two highest amplitude modes which span the frequency range of the δ Sct pulsations, we find $Q = 0.019$ for the 32.0888-d^{-1} frequency and $Q = 0.015$ for the 39.8553-d^{-1} frequency. Comparing these with model 4.4 in Stellingwerf (1979) suggests that modes in the δ Sct star range in radial overtone between $n \sim 2-4$. This is a narrow range of overtones, and the number of observed frequencies in the range requires most of the associated modes to be nonradial. At first glance, TIC 5724661 seems to be a relatively hot δ Sct star, and since hotter stars tend to pulsate in higher radial overtones (Breger & Bregman 1975), $n \sim 2-4$ radial overtones are not unexpected. However, we are also cognizant of the fact that the temperature estimate given in the TIC may be inflated due to an unresolved sdB companion; more details are discussed in Section 5.

Three of the peaks are nearly equally spaced in frequency: 34.3520, 35.0681 and $35.7721\,\mathrm{d}^{-1}$. The separations between pairs of these peaks are 0.7161 ± 0.0025 and $0.7040 \pm 0.0024\,\mathrm{d}^{-1}$; these separations themselves differ only by $0.012 \pm 0.003\,\mathrm{d}^{-1}$. Despite this small difference, the formalism provided in Dziembowski & Goode (1992) appears to suggest that this triplet does not arise from rotational splitting. However, if we *do* assume rotational splitting, we can crudely estimate $P_\mathrm{rot} = 1.4$ d (neglecting the Ledoux rotational splitting constant $C_{n,\ell}$. Moreover, because we know that the binary contains a δ Scuti star, we can use the illustrative values $\log g = 4.3$ and $M \sim 2\,\mathrm{M}_\odot$ to derive a crude radius estimate of $R \sim 1.6\,\mathrm{R}_\odot$. These values, along with the rotational period estimate, predict that $v_\mathrm{eq} = 60\,\mathrm{km\ s^{-1}}$. The spectroscopic estimate of $v \sin i$, 39.9 ± 0.9 km s^{-1}, suggests that the rotational axis of the star is tilted $\sim 40°$ with respect to our line of sight (here, we use the convention that 0° is parallel to our line of sight). We emphasize that these are only first-order estimates; further analysis and modeling (discussed in Sections 5 and 6) can better constrain these parameters.

Most A stars with $v_\mathrm{eq} \lesssim 100\,\mathrm{km\ s^{-1}}$ are either Am or Ap stars, meaning they exhibit strong metal lines (the distinction arises from the presence of a strong dipole magnetic field in Ap stars; see, e.g., Murphy 2014). So, we would expect TIC 5724661 to show abundance anomalies when examined at high spectral resolution, most probably of the Am kind, as nearly half of A stars near this temperature are Am stars (Smith 1973). However, as discussed in Section 4, no abundance anomalies were detectable in our spectra; we may need a data with a higher spectral resolution to see such anomalies. More

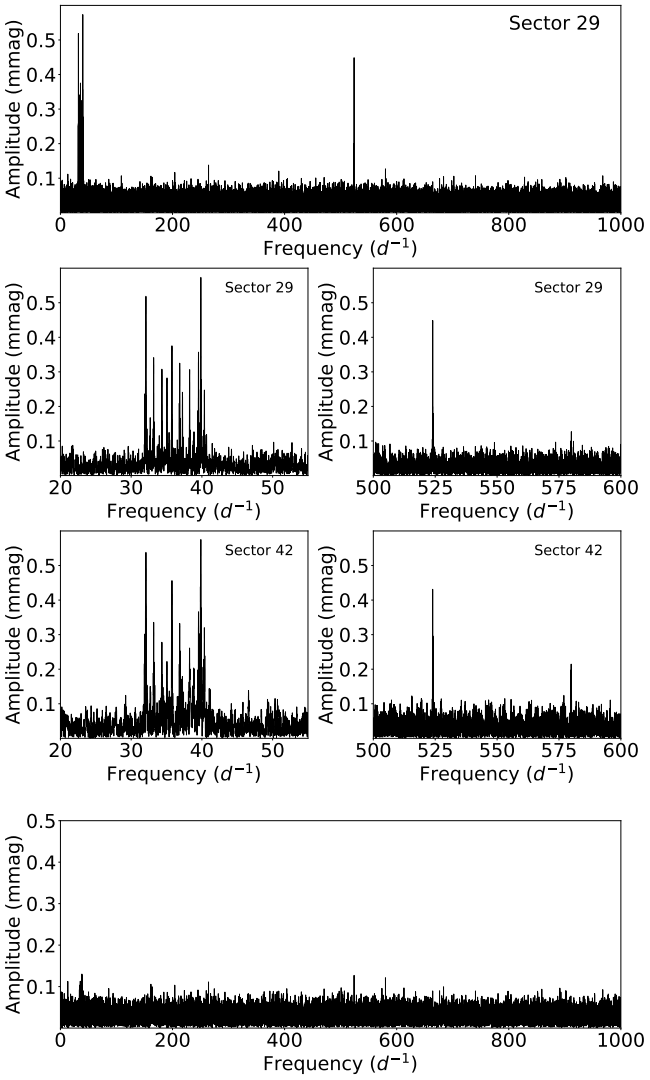

Figure 2. The top panel shows the Fourier amplitude spectrum to 1000 d^{-1} from the Sector 29 light curve; there are no significant peaks between 1000 d^{-1} and the Nyquist frequency, 2160 d^{-1}. The second panel zooms into a cluster of peaks in the δ Sct frequency range between $20 - 55\,d^{-1}$, along with a single, high-frequency peak at 523.99 d^{-1} (6.065 mHz). The third panel shows the δ Scuti and high-frequency pulsations observed in Sector 42; the peak at 579.85 d^{-1} (6.711 mHz) increases in prominence between Sectors 29 and 42. The bottom panel shows the Fourier spectrum of the residuals after a non-linear least-squares fit of the 13 highest-amplitude δ Sct peaks and the peak at 523.99 d^{-1} (from the sdB star) is subtracted from the data.

evidence against the idea that the 523.99 d^{-1} pulsation arises from a roAp star is the fact that this frequency is more than twice the theoretical acoustic cutoff frequency for such a star. While supercritical roAp pulsations have been observed, none of them have deviated from the cutoff as strongly (see, e.g., Holdsworth et al. 2018, and references therein).

Table 3. A non-linear least squares fit of 13 δ Sct frequencies and 1 sdBV frequency to S29 data. The zero point for the phases, $t_0 = 2459100.41122$, is the center in time of the data.

frequency d^{-1}	amplitude mmag ± 0.024	phase radians
31.9317 ± 0.0021	0.246	-1.534 ± 0.102
32.0888 ± 0.0010	0.522	-2.884 ± 0.047
32.7019 ± 0.0032	0.160	-1.931 ± 0.151
33.1820 ± 0.0015	0.341	1.555 ± 0.071
34.3520 ± 0.0017	0.300	0.531 ± 0.081
35.0681 ± 0.0019	0.267	-1.539 ± 0.091
35.7721 ± 0.0014	0.362	-0.086 ± 0.067
36.8673 ± 0.0015	0.330	2.064 ± 0.073
37.2562 ± 0.0021	0.243	-1.097 ± 0.100
38.2666 ± 0.0016	0.314	3.071 ± 0.077
39.5224 ± 0.0014	0.356	-2.691 ± 0.068
39.8553 ± 0.0009	0.585	1.304 ± 0.042
40.3589 ± 0.0020	0.258	-1.756 ± 0.094
523.9899 ± 0.0011	0.449	2.917 ± 0.054

Another possible explanation for the high-frequency pulsation observed at 524 d^{-1} is a white dwarf. Many white dwarfs are known to pulsate in this frequency regime, with frequencies associated with g modes, as opposed to p modes, which underlie the oscillations in sdBV$_r$ stars (Winget & Kepler 2008). However, as shown in Figure 2, the amplitude of the high-frequency oscillation is 0.394 mmag. This is 0.036% of the entire system's light. Using $L = 4\pi\sigma R^2 T^4$, and adopting illustrative values of 0.01 $R_\odot$ for the white dwarf radius and 20 000 K for the temperature, we expect the luminosity ratio of the two bodies to be 10^{-3}, implying the white dwarf pulsates with an amplitude that is $\sim 35\%$ of its luminosity. Typical WD pulsation amplitudes are between 1 and 2% (Winget 1998); as a result, this is not a plausible option able to explain our observations.

Finally, we evaluate the possibility that there is some foreground or background contamination in the *TESS* light curve, due to the large size of its pixels. The *Gaia* eDR3 catalog (Gaia Collaboration et al. 2021) shows that TIC 5724661 only has one nearby star within 80", and this star has $m_G = 19.5$ – too faint to exhibit pulsations of the amplitude that we observe. Moreover, this nearby star's *Gaia* BP−RP value is 1.74, suggesting that this is an extremely cool star that should not be able to pulsate at all (Andrae et al. 2018). Moreover, the Renormalized Unit Weight Error (RUWE) for TIC 5724661 is 1.482 – which is significantly greater than the expected

value of 1; relatively large RUWE values can be used as a proxy for binarity (see, e.g., Belokurov et al. 2020). As a result, we can safely discount the possibility of contamination by another source and focus on the possibility of a hot compact companion.

We thus conclude that this high-frequency mode likely arises from a p mode sdBV$_r$ star. Constraints on its mass are discussed in Section 4, its temperature in Section 5, and its evolutionary history in Section 6.

4. SPECTRAL ANALYSES

To study the spectra we obtained, we conducted two analyses—one to establish constraints on the radial velocity variations, and hence on the mass of a potential unseen sdB companion, and another in which we directly searched for spectral signatures to check the chemical composition of the A star and identify any peculiarities.

First, we used the lack of detectable RV variations to constrain the mass of a potential companion. We fit for the K velocity, phase, and γ velocity of the RV curve for each of 10^6 trial periods evenly spaced in logarithmic space between 0.1 and 1000 d, all assuming circular orbits. To be conservative when generating our constraints, we multiplied the LSD uncertainties (described in Section 2) by 1.5 and input those as the argument `sigma` to the `curve_fit` function in `scipy`. For each trial period, we then calculated an upper limit to the value of the mass function using the best-fit K value plus twice its derived uncertainty. Finally, we solved for the corresponding limit to the mass of a potential companion by using the upper limit on the value of the mass function and an assumed mass for the A star of $2M_\odot$. This was done for each of three assumed orbital inclinations of 30°, 60°, and 90°. A plot of the derived upper constraints for a potential companion is given in Figure 3. The data suggest that any sdB star companion is more likely to be in an orbit longer than ~ 150 d. However, there are cases involving low inclination angles that could harbor either a short- or medium-period sdB star (e.g., 35-80 d). There is also the possibility the orbit is eccentric, which may lead to inauspicious locations along the orbit when the radial velocities were measured. The region of parameter space resulting in medium periods is explored further in Section 6.

We then turned our attention to directly analyzing the spectrum to ascertain more about the nature of the A star. We began by summing the seven TRES spectra into one, as there were no significant radial velocity differences among them. The summed spectrum had a S/N of about 65 and was, just like in Section 2.2, compared to model atmospheres using ATLAS9 (Castelli & Kurucz 2004) and SPECTRUM (Gray & Corbally 1994). An

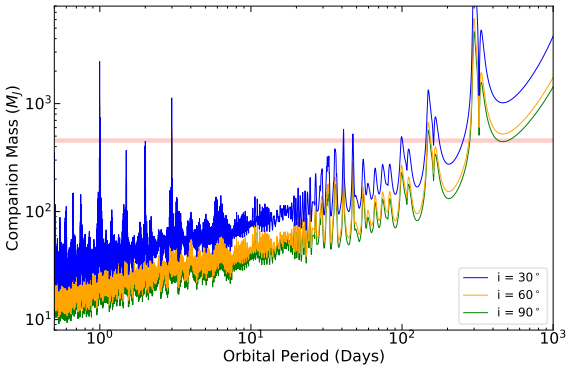

Figure 3. Upper limits on the mass of a potential companion to a 2 $M_\odot$ star that are derived from our RV measurements for a range of assumed orbital inclinations. The shaded red region indicates the range of masses of the sdBs that resulted from the modeling of various evolutionary scenarios (described in Section 6). It is clear that the derived constraints are more stringent for periods $\lesssim 35$ d. There exist islands of marginally acceptable binary periods between 35 and ∼60 d; more probable periods lie near 150 and ∼ 300 d. Spikes represent locations at which we do not possess any information on the mass of a potential companion, as a result of our observing cadence. The narrow spikes below 3 d are aliases of the 1 d observing windows.

atmosphere with $T_{\rm eff} = 8000$ K, $\log g = 4.0$, [M/H]=0, broadened to $v \sin i = 40$ km s^{-1} gave a good fit to the summed spectrum. A search for chemical peculiarities indicative of a magnetic A star yielded a null result, with the possible exception of a somewhat narrow Ca K line at 393.366 nm. Likewise, searches for He lines in the summed spectrum caused by a possible sdB companion remained negative. This latter non-detection could be explained through a pure-H atmosphere, which may arise from chemical differentiation processes in the sdB: Hunger & Kudritzki (1981) and Latour et al. (2018) suggest that processes such as gravitational settling, stellar winds (for hotter subdwarf stars), and convective instability can cause the He abundance to deviate from what is expected. Or, this could simply be a consequence of such a companion being some 2.5 magnitudes fainter than the δ Scuti star in the optical (cf. Figure 4).

5. SPECTRAL ENERGY DISTRIBUTION

The spectral energy distribution (SED) obtained from the Vizier portal (Ochsenbein et al. 2019) exhibits an excess in the ultraviolet flux in both the Galex NUV and FUV bands (see Fig. 4). Thus, we fit the SED with a model for the summed spectra from an A star and an sdB star to further test the possibility of an unresolved long-period hot sdB companion to the A star.

We used a custom implementation of the Markov Chain Monte Carlo (MCMC) algorithm to estimate parameters for the temperatures and radii of the two potential stars in the system. Extinction was accounted for by using $A_V \simeq A_G = 0.357$ (obtained from *Gaia* DR2), along with the analytic formulas provided in Cardelli et al. (1989). The distance to the source was fixed at 727 pc, based on the *Gaia* parallax measurements given in DR2 (Prusti et al. 2016; Brown et al. 2018).[3] The Vizier data points were fit with summed model Kurucz spectra of an A star with fixed $\log g = 4.3$ and an sdB star with fixed $\log g = 5$ (Castelli & Kurucz 2004). We set the priors on the A star to be $1\,R_\odot < R < 2.5\,R_\odot$, with $7000\ \mathrm{K} < T_{\rm eff} < 11000\ \mathrm{K}$. The sdB star's radius was sampled logarithmically and constrained to be within $0.1 < R < 1\,R_\odot$, with $22000 < T_{\rm eff} < 38000$ K.

To ensure confidence in our assumption that fixing the value of $\log g$ would not significantly impact the SED model values, we used the Tübingen NLTE model spectra to vary $\log g$ for the sdB companion. This parameter was varied from $5 \leq \log g \leq 6.5$ (Werner et al. 2012), leading to only insignificant differences in the derived SED, with the largest being a few parts per thousand of the largest SED flux value. Therefore, we were confident that we could fix the values of $\log g$ for both stars in the system, as described above, without losing any critical information. This assumption was borne out when we plotted the posterior distribution for this parameter, which was essentially flat – suggesting that the SED is highly insensitive to this parameter. As a result of this degeneracy, we constrained $\log g$ through stellar evolution modeling – see section 6 for more details.

We allowed the MCMC to run for 1 million steps. The best-fit parameters for the system are presented in Table 4, along with their associated uncertainties. Figure 4 shows the best-fit spectrum superposed on the available data points. The fit is good, with a reduced χ-squared value close to unity. A corner plot illustrating the posterior distributions and their correlations between parameters is shown in Figure 5; all parameters are somewhat correlated. There exists a strong correlation between the radius and effective temperature for the sdB star, as expected – since its radiation dominates the observed SED only in the UV region of the spectrum. We do not show the posterior distributions for $\log g$, as these are flat and do not yield new information.

[3] Since *Gaia* eDR3 (Gaia Collaboration et al. 2021) does not include a solution for A_G, we used the parallax from DR2 to ensure consistency with the value we used for A_G. The eDR3 parallax solution yields a distance of 611 pc.

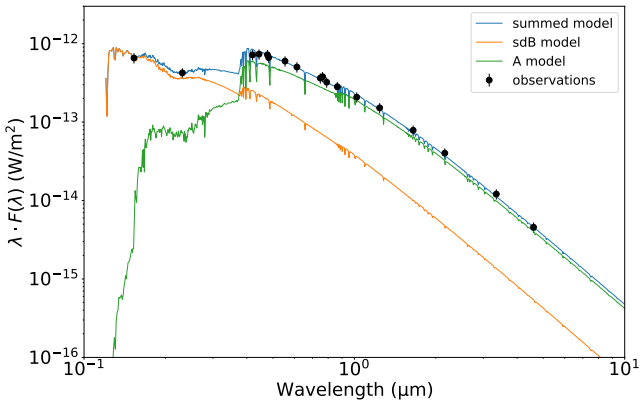

Figure 4. SED plot for TIC 5724661 (black points), where the smooth curves are the model fits using Kurucz (Castelli & Kurucz 2004) spectra for the sum of the A star and the inferred sdB star; these have been corrected for interstellar extinction. The fits are described in detail in the text. The green curve is for the A star alone, while the orange curve represents the flux of a companion sdB star. It is evident that the sum of the models for an A star and an sdB star can explain the observed SED much better than either would on their own. This lends credence to our claim that there is a compact, hot body orbiting the A star.

Table 4. Derived values for $T_{\rm eff}$ and R for both stars.

Parameter	Value
$T_{\rm eff}$ - A star	8630^{+280}_{-260} K
R - A star	$1.69 \pm 0.05\ R_\odot$
$T_{\rm eff}$ - sdB star	29500^{+5100}_{-4900} K
R - sdB star	$0.23^{+0.09}_{-0.06}\ R_\odot$

These fitted parameters for the putative sdB star agree with what is expected for the temperature of such a pulsating star. Figure 51 of Heber (2016) shows a demarcation between short- and long-period sdB pulsators, with the former having higher temperatures and $\log g$ values. Our results are thus reassuring, insofar as our inference of a pulsating sdB companion based on the observation of a short period pulsation in the *TESS* data is bolstered by the value of our best-fit temperature. However, what is unique about this sdB star is that it could potentially lie in a little-explored region of binary parameter space, as it could possibly have an orbital period that is too long to suggest formation via common-envelope evolution, and too short to evolve via stable, fully conservative mass transfer.

6. EVOLUTIONARY ANALYSIS

Most evolutionary channels leading to the formation of hot subdwarfs rely on a red-giant progenitor that is rapidly stripped of its deep, hydrogen-rich envelope as a

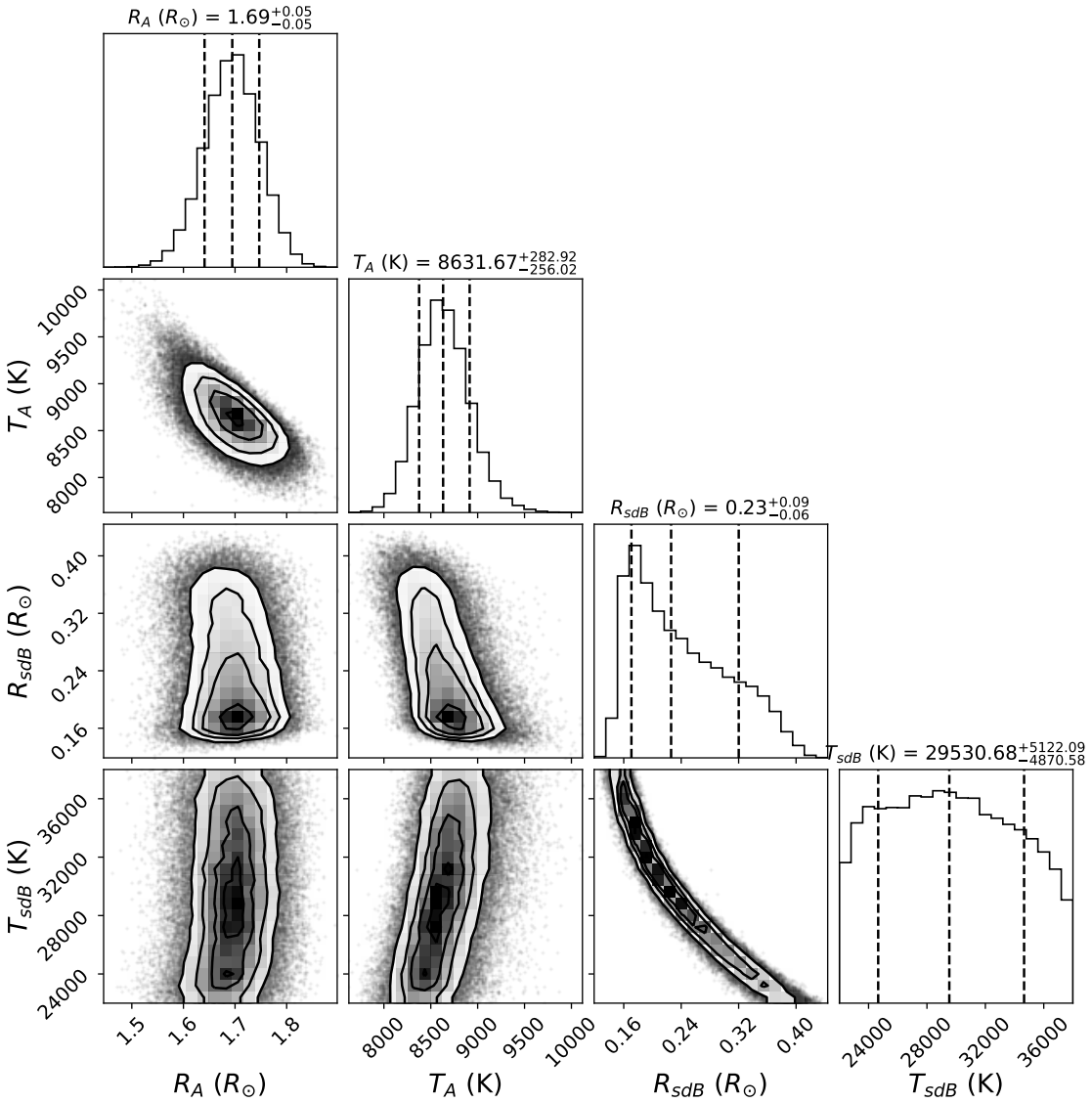

Figure 5. Posterior distributions for the parameters of TIC 5724661. This corner plot shows the best-fit parameters and the correlations between the parameters derived through an MCMC fitting code. Dashed vertical lines, from left to right, represent the 16th percentile, median, and 84th percentile. The distribution for the temperature of the sdB star seems to fall off at high temperatures, suggesting that a $T_{\rm eff}$ close to 29 000 K is most likely. There exists a strong degeneracy between the $T_{\rm eff}$ and the radius of the sdB star, as expected, given the limited region of the SED where the sdB star likely dominates the system light.

result of binary interactions. Once the red giant's core is exposed, it rapidly evolves along the extreme horizontal branch (EHB; see Heber 2016, and references therein).

We have adopted the following working definitions regarding hot subdwarfs and their key properties:

1. sdBs burn helium (He) in their cores, and may also undergo α-channel burning of the newly-created carbon in the core (leading to the creation of oxygen). This phase persists for tens of Myr, during which time the radius remains roughly constant.

2. sdO stars have a well-defined carbon-oxygen (CO) core, with helium burning occurring in a shell around the core. Simultaneous hydrogen burning occurs in a thin layer near the surface. This phase is typically shorter than the sdB phase (by a factor of 2 to 3), and the radius also remains roughly constant during this phase.

3. sdA stars have poorly constrained properties. Their true nature remains uncertain because there may be a variety of processes leading to their for-

mation. This remains an important open question, but sdA stars are not of importance for this work.

A large fraction of sdBs are found in binary systems, and the majority of these are found in short-period binaries ($P_{\rm orb} \lesssim 5\,{\rm d}$) with low-mass companions (e.g., M stars). There clearly exists a selection effect favoring the discovery of short-period eclipsing binaries due to strong illumination effects and deep eclipses, especially for large orbital inclinations. While there is extensive observational evidence for sdBs in short-period binaries, there have been many fewer examples of observed long-period binary systems ($P_{\rm orb} \gtrsim 100\,{\rm d}$). Moreover, TIC 5724661 has an inferred period that is significantly longer than many other observed sdB stars, falling in a sparsely populated region of parameter space. This could possibly imply a deficiency in our understanding of the (binary) hot subdwarf formation process.

6.1. *Formation of sdB stars*

The formation and evolution of hot subdwarf stars has been studied extensively by Mengel et al. (1976), Castellani & Castellani (1993), Dorman & Rood (1993), Han et al. (2002, 2003), Justham et al. (2011), Schindler et al. (2015), and Senhadji (2019). Han et al. (2003) investigated various evolutionary channels that lead to the formation of sdB stars and concluded that sdBs in tight binaries ($P_{\rm orb} \lesssim 5\,{\rm d}$) were probably formed as a result of common envelope evolution. They also showed that wide systems containing sdBs ($P_{\rm orb} \gtrsim 100\,{\rm d}$) were likely the result of stable conservative Roche lobe overflow. They also showed that wide systems containing sdBs ($\rm P_{orb} \gtrsim 100$ d) were likely the result of stable Roche lobe overflow onto a white dwarf companion (they did not model main-sequence accretors).

For common envelope evolution to produce an sdB, a red giant whose mass is at least 2 to 3 times greater than that of its companion must overflow its Roche lobe. The rapid shrinking of the giant's Roche lobe as it loses mass causes dynamically unstable mass transfer, forcing the accreting companion to spiral inside the giant's envelope (see, e.g., Webbink 1976). If the change in the orbital energy is sufficient to unbind the envelope, then the giant's envelope can be expelled from the binary system on the order of hundreds of years (Xiong et al. 2017). If a merger can be avoided, the companion emerges in a tight, circular orbit (periods of hours to days) around the stripped core of the red giant. This stripped core can then evolve onto the EHB and become an sdB/O.

As noted by Han et al. (2002), it is possible for a hot subdwarf to be formed as a result of (stable) mass transfer from a giant donor to a white dwarf companion as the donor evolves up the red giant branch (RGB). Because the donor is already a giant at the onset of mass transfer and because orbits widen as a result of mass transfer, the sdBs are typically formed in wide binaries with orbital periods of hundreds to thousands of days (see, e.g., Vos et al. 2019 and references therein). It is also possible to form sdB/O binary stars via stable, non-conservative mass transfer to main-sequence accretors. While we know that mass transfer is non-conservative based on an analysis of Algol-related binaries (Eggleton 2000), we do not have a good constraint on systemic mass loss (i.e., the fraction of mass ejected from the binary). An extensive grid of progenitor models was calculated by Senhadji 2019 of potential progenitors of hot subdwarfs, under the assumption of partially non-conservative, stable mass transfer. This work suggests that sdB-containing binaries could have values of $P_{\rm orb}$ between ≈ 5 to 500 days. Thus, they naturally bridge the gap in $P_{\rm orb}$ between sdBs formed as a result of common envelope evolution and those formed from purely conservative mass transfer. The question now arises as to whether we can produce sdBs with $P_{\rm orb} \gtrsim 70\,{\rm d}$ and $T_{\rm eff} \approx 30\,000$ K, as we have estimated for TIC 5724661.

6.2. *Evolutionary Simulations*

In trying to determine the initial conditions needed to reproduce the inferred properties of TIC 5724661, we created a highly focused grid of evolutionary tracks using the `MESA` binary stellar evolution code (Paxton et al. 2011, 2013, 2015, 2018, 2019). We had previously used `MESA` to successfully explain the current evolutionary state of MWC 882 (Zhou et al. 2018) – which itself will evolve to become an sdB – and subsequently computed a grid of about 3500 models whose initial conditions were chosen so as to optimize the likelihood of the formation of sdBs in wide binaries (Senhadji 2019). Those models assumed varying degrees of non-conservative mass loss and produced sdBs with a wide range of effective temperatures (20,000 K $\lesssim T_{\rm eff} \lesssim$ 50,000 K). Guidance from this grid allowed us to optimize our computations by concentrating on a much smaller grid corresponding to cases of highly non-conservative mass transfer only.

The evolutionary tracks in this focused grid were computed using `MESA` version r10108. The sdB progenitor (i.e., the primary) was assumed to have a typical Population I metallicity ($Z = 0.02$), the atmosphere was approximated by a simple boundary condition ($\tau = 2/3$), and the local mixing-length ratio was set equal to 2. We applied the default parameters for both the Reimers wind formula (Reimers 1975) and the Blöcker wind formula (Bloecker 1995). We tested a reasonable range of other values for these parameters and found that they had a negligible effect on the results. By far, the most

important factors influencing the evolution, other than $M_{1,0}$, $M_{2,0}$, and $P_{\rm orb,0}$ (i.e., the initial mass of the primary, secondary, and orbital period, respectively), were the parameters α and β (Tauris & van den Heuvel 2006). The parameter α is the fraction of the mass lost from the primary (donor) and then ejected from the binary, carrying away the specific angular momentum of the primary. Similarly, β is the fraction of the mass transferred from the primary (donor) to the secondary (accretor) that is subsequently lost from the binary, carrying away the specific angular momentum of the secondary.[4] (Another interpretation of β is the fraction of mass lost from the binary *after* it has crossed the L1 point.) To eliminate one extra dimension of parameter space in our computations, we set $\alpha = 0$. The main justification for this strategy is our (empirical) finding that the value of $\alpha+\beta$ had a much greater impact on the evolution than did various combinations of those parameters corresponding to the same sum. So, our choice of β determined the degree of non-conservation of mass transfer.

Both binary stars are evolved contemporaneously with `MESA`. It is important to follow the evolution of the secondary as it accretes mass because the secondary can expand to fill its Roche lobe.[5] The reasons why the secondary can potentially fill its Roche lobe are as follows: (1) if the mass accretion rate onto the secondary ($\dot{M}_2$) is too high, it can expand adiabatically; or, (2) if the mass of the secondary were to increase substantially on a short timescale, then it could evolve to become a giant (and fill its Roche lobe) before the primary (donor) has had a chance to complete its sdB phase.[6] In either case, `MESA` halts any further computation. In order to increase the chances that the primary evolves through the sdB phase, we typically attenuated the mass accretion rate onto the secondary by requiring that $\beta \gtrsim 0.8$ (recall that $\dot{M}_2 = -(1-\beta)\dot{M}_1$). Obviously, if mass transfer is fully non-conservative ($\beta = 1$), the secondary is not likely to fill its Roche lobe until long after the sdB phase is complete (i.e., if the primary evolves along the EHB).

Finally, we note that the requirement that β be large implies that the orbital periods cannot be nearly as large as those found by Han et al. (2002), who considered mass accretion from a giant donor onto a white dwarf. Other than starting from a much lower period at the onset of mass transfer compared to their models, the main reason stems from the fact that for large values of β, systemic mass loss will ensure that a significant fraction of the binary's orbital angular momentum ($\delta J/J$) is carried out of the system. Because J^2 is proportional to the binary separation, the loss of angular momentum will cause the orbit to shrink relative to what would have been obtained had the evolution been fully conservative.

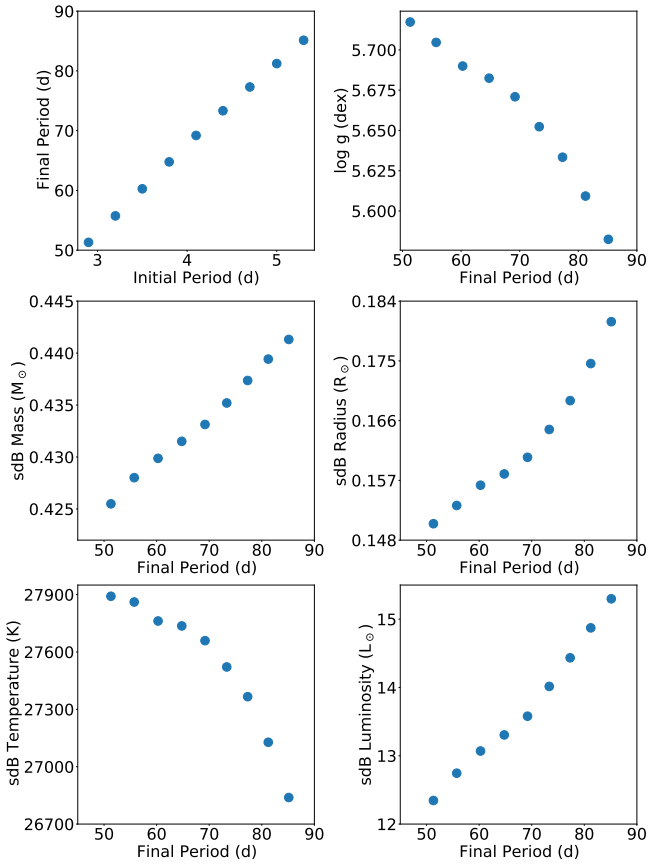

Figure 6. A multi-panel plot showing how the various properties of a representative sdB star depend on the initial period of the binary. The initial mass of the sdB star's progenitor was 3.25 $M_\odot$, its companion's initial mass was 1.7 $M_\odot$, and β was fixed at 0.95. The plots show that for larger initial periods, the sdB star's mass, radius, and luminosity increase, as does the final orbital period; however, its effective temperature and log g decrease.

6.3. *Results*

Using the methods described in the previous subsection, we have shown that the inferred observational parameters for TIC 5724661 are reproducible, as long as we are willing to accept a large fraction of non-conservative mass transfer. By adjusting the properties of the primordial binary such that $M_{1,0} \approx 3.5 \pm 0.3$ $M_\odot$, $M_{2,0} \approx 1.6 \pm 0.3$ $M_\odot$, and $P_{\rm orb,0} \approx 4 \pm 2$ d, with $\beta \gtrsim 0.8$, we were able to produce multiple tracks for

[4] Both of these cases correspond to the "fast Jeans' mode" of angular momentum dissipation

[5] If the primary is still transferring mass, the resulting evolution might lead to a merger.

[6] Moreover, with respect to TIC 5724661, this would be especially problematic because the giant would be more luminous than the sdB star (contrary to observations), and it would not exhibit δ-Scuti-like pulsations.

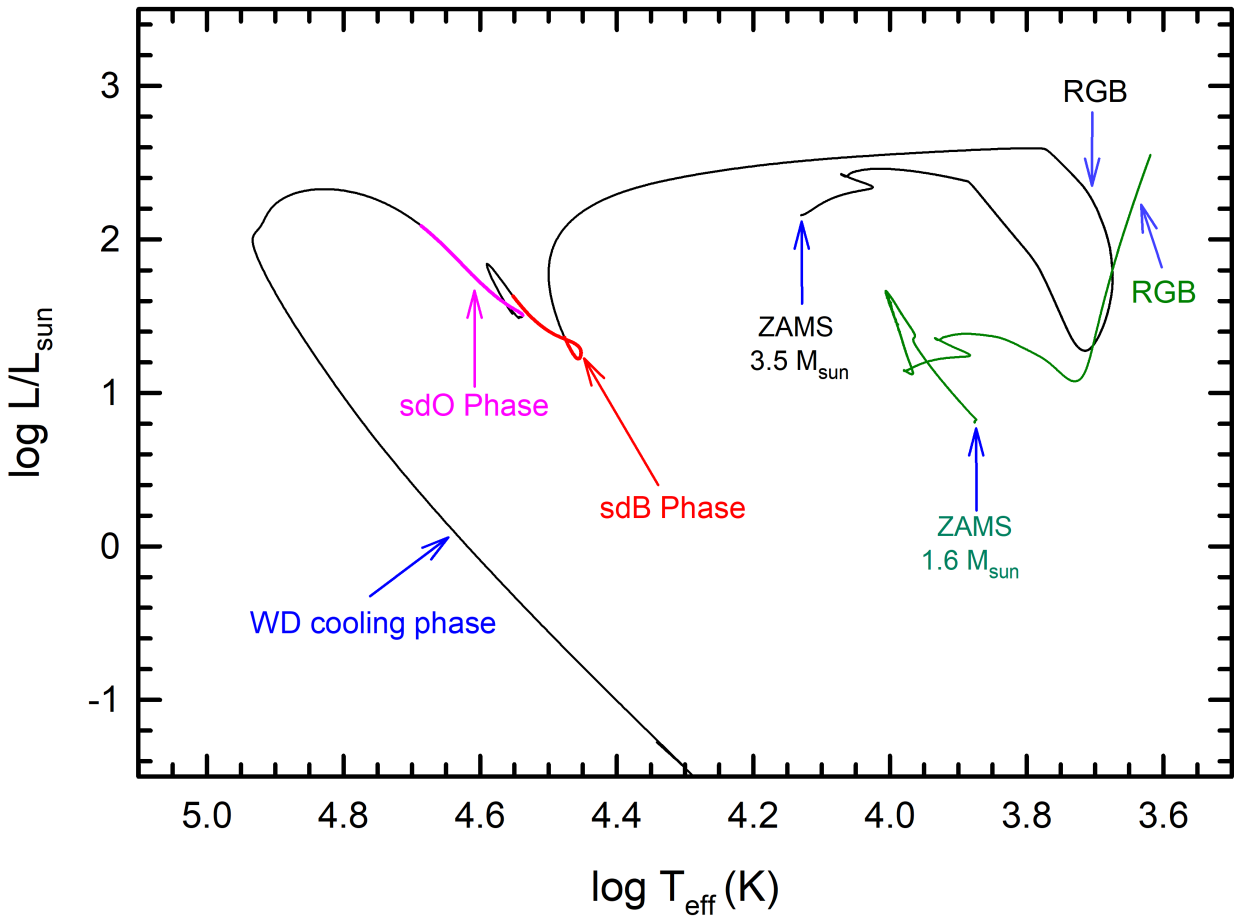

Figure 7. Evolution of a representative sdB from the zero-age main sequence (ZAMS) to the final WD cooling stage in the HR diagram (solid black line); note that the pre-main sequence has been removed for reasons of clarity. The ZAMS progenitor star has a mass of 3.5 $M_\odot$ and an approximate solar metallicity ($Z = 0.02$). Mass transfer is initiated in the Hertzsprung Gap and continues as the progenitor ascends the Red Giant Branch (denoted as RGB). Mass transfer ceases once its mass is reduced to 0.470 $M_\odot$ and this stripped core evolves along the horizontal branch until it reaches the sdB phase. This phase persists for almost 80 Myr (red curve) before the hot subdwarf evolves through the sdO phase (magenta curve) for an additional 40 Myr. After H-burning near the surface is quenched, the star cools as an electron-degenerate white dwarf. The evolution of the companion star is also shown (solid green curve). Its initial mass is 1.6 $M_\odot$ and undergoes a phase of rapid accretion before it reaches thermal equilibrium (after mass transfer has ceased) and evolves normally as a 1.9 $M_\odot$ star. The star ascends the RGB and the evolution is halted once the star is large enough to fill its Roche lobe.

which the sdB's effective temperature was in the range of 27,000 and 35,000 K, its $\log g$ was between 5.4 to 5.8, and the final orbital period was between 30 and 80 d. These results are in general agreement with the inferred properties of TIC 5724661 shown in Table 4.

Figure 6 provides an example of how the predicted properties of the sdB depend on one of the dimensions of initial parameter space (i.e., $P_{\rm orb,0}$). For this example, the initial conditions for the primordial binary were $M_{1,0} = 3.25\,M_\odot$, $M_{2,0} = 1.7\,M_\odot$, with $\beta = 0.95$. Not surprisingly, increasing the initial period serves to monotonically increase the final period. Increasing the initial period implies that the donor star (primary) will be more evolved at the onset of mass transfer. This also implies an increased mass, radius, and luminosity of the sdB, but lowers its eventual effective temperature.

The HR diagram for one of our representative cases that very closely reproduces the properties of the sdB in TIC 5724661 is shown in Figure 7. The sdB progenitor has a mass of 3.5 $M_\odot$, with a Population I metallicity of $Z = 0.02$; the value of β was set equal to 0.9. Mass transfer commences in the Hertzsprung Gap and continues

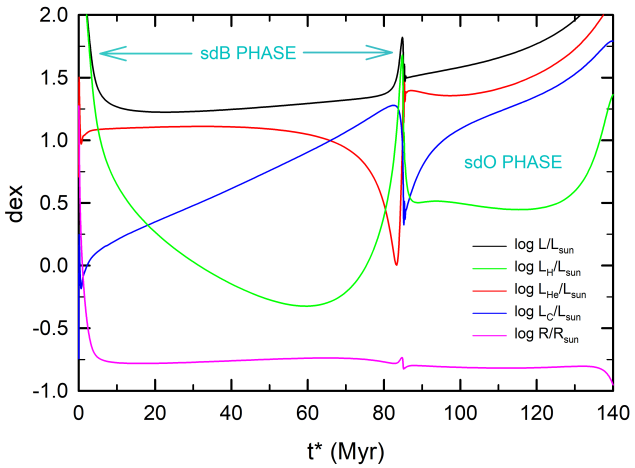

Figure 8. Evolution of the bolometric luminosity, individual nuclear luminosities, and radius of the representative hot subdwarf as a function of time. Note that $t^* = 0$ has been chosen to approximately coincide with the end of the RGB phase ($t^* = t - 211.25$ Myr). The sdB phase persists for nearly 80 Myr, during which time helium is continuously depleted due to triple-α burning and the fusion of carbon into oxygen (α-channel burning). Once a CO core forms and the subdwarf experiences He-shell flashes, it enters into a shorter-lived sdO phase. For each phase, the radius of the subdwarf is approximately constant.

as the progenitor ascends the Red Giant Branch. Mass transfer rates from the donor sometimes exceeded 10^{-5} $M_\odot$/yr, resulting in a large fraction of the giant donor's hydrogen-rich envelope being lost rapidly to the interstellar medium. Mass transfer ceases once the highly mass-depleted envelope collapses and no longer fills its Roche lobe. After this happens, the primary is essentially a hot helium core of mass 0.470 $M_\odot$, and it contracts very rapidly (in $\sim 3\times10^5$ yr) along the horizontal branch before entering the long-lived sdB phase ($\sim$ 100 Myr); the sdB phase is denoted by the red portion of the evolutionary track in Figure 7.

We define this phase to extend from the point at which helium burning has increased the carbon mass fraction at the star's center by 1% above its primordial value to the point when a (convective) CO-rich core first emerges. It is at this juncture that late-stage He flashes occur and persist briefly before the hot subdwarf enters the sdO phase (the magenta curve). During this stage, the CO core can grow substantially in mass as the result of He-burning in a shell surrounding the core. Once the CO core has grown to reach about 95% of the total mass, the radius of the hot subdwarf contracts rapidly – signaling the termination of the sdO phase. Subsequently, the thin H-rich layer near the surface can be compressed and concomitantly heated as a result of the envelope's rapid contraction. This temperature increase is often high enough for the star to undergo one or more cycles of H-shell flashes (see, e.g., Nelson et al. 2004, and references therein). Once the H-burning is quenched, the star descends onto the white dwarf cooling track.

The solid green curve in Figure 7 shows the evolution of the secondary star (i.e., the accretor). Its initial mass is 1.6 $M_\odot$, and it undergoes a phase of rapid accretion before reaching thermal equilibrium (after mass accretion has ceased). It reaches a maximum mass of 1.9 $M_\odot$ and evolves to become a subgiant before ascending the RGB. `MESA` halts the evolution once the star fills its Roche lobe. If we continued to follow the evolution, we would see a subsequent phase of common-envelope evolution resulting in the formation of a double-degenerate binary. The expected end product would be a 0.47 $M_\odot$ white dwarf (the sdB component) in close orbit with a lower mass helium white dwarf (the core of the giant).

Figure 8 provides more detail with respect to the sdB and sdO evolutionary phases. It shows the temporal evolution of the nuclear luminosities from the H-, He-, and C-burning channels, and the evolution of the surface luminosity[7] and radius. The high luminosities seen near $t^* = 0$ ($\equiv t - 211.25$ Myr) arise from the evolution of the primary star while it is a red giant. After the star settles into the sdB phase, its radius remains approximately constant for ~78 Myr. Initially, He-burning accounts for most of the luminosity, but as more and more carbon is created, α-channel capture occurs, converting some of the carbon into oxygen. As both the luminosity and radius approach a local maximum, a convective core (≈ 0.1 $M_\odot$) of CO is formed, and the hot subdwarf thermally relaxes, leading to a brief phase of He-shell flashes. The subdwarf subsequently enters the sdO phase, during which time the radius is reasonably constant over $\approx$ 40 Myr. From a theoretical perspective, we can think of the sdB and sdO phases as being long-lasting ($>$ 10 Myr) and quasi-quiescent. The hallmark of the sdB phase is He-burning in the core. On the other hand, for the sdO phase, He-burning primarily occurs in a shell surrounding the CO core. According to conventional wisdom, $T_{\rm eff}$ is lower for sdB stars than for sdO stars. Figure 7 shows this holds for our representative case, but this need not always be true (Senhadji 2019).

Our models show that the mass of the A star companion (i.e., the secondary) could lie in the range of $\approx$1.8 to 1.9 $M_\odot$. The main reason that the secondary masses

[7] Note that the sum of the nuclear luminosities may not equate to the surface luminosity. This difference is due to the gravothermal luminosity, whose magnitude is not shown.

are so large is that: (i) the intial mass ratio ($M_{2,0}/M_{1,0}$) must be sufficiently high at the onset of mass transfer ($\gtrsim 0.4$) to avoid dynamical instability (otherwise, this could lead to a merger); and, (ii) $M_{1,0}$ must be $\gtrsim 3 M_\odot$ so that the primary has a chance to initiate core He-burning after departing the Red Giant Branch.[8] According to the main sequence models of Eker et al. 2015, a 1.9 $M_\odot$ solar-metallicity model has a luminosity of about 15 $L_\odot$, $T_{\rm eff} \approx 8000$ K, and $R \approx 2\ R_\odot$. Its inferred spectral type is A2.5V. These values are in line with the inferred values shown in Table 4.

7. CONCLUSIONS

In this paper, we present strong evidence for the true nature of TIC 5724661: a main-sequence A star with an inferred long-period sdBV$_{\rm r}$ star in orbit around it. First, we used radial velocity data to show that the putative hot subdwarf companion must have a period longer than a few tens of days. We then fit the spectral energy distribution using an MCMC code to constrain the parameters of the two stars in the system and provide fairly compelling evidence that this star is indeed an sdB star. To determine whether such sdBs can be produced using non-common-envelope formation channels, we modeled this system with MESA and demonstrated that we can readily produce such stars, as long as there is a high degree of non-conservative mass transfer. We expect that the current A star in TIC 5724661 could have accreted perhaps $\sim 10\%$ of the mass lost from the red giant progenitor of the sdB, implying a final mass of 1.9 $M_\odot$. This would ensure that this star, which exhibits δ Scuti pulsations, is an A star (A2.5V). A more limiting constraint on the minimum value of $P_{\rm orb}$, perhaps via more spectroscopic observations, may serve to either strengthen or invalidate our evolutionary model.

Our work, therefore, adds more observational evidence for intermediate- and long-period binaries with an sdB component (for others, see, e.g., Vos et al. 2019, and references therein). Previously, many observed sdB binaries were found to have extremely short periods and were therefore thought to have passed through a common-envelope phase. Our work lends observational evidence to the fact that such common envelopes are not necessary to form sdB stars (see, e.g., Senhadji 2019 for a set of intermediate- to long-period sdB formation models), especially ones pulsating in high-frequency p modes.

Finally, this paper – which utilizes the new *TESS* 20-second cadence data – further emphasizes the power of *TESS* for precision asteroseismology. The continuous, short-cadence nature of *TESS* data enables the detection and study of objects and pulsations that ground-based observatories would struggle to identify and characterize. As a result, we were able to identify and derive a precise frequency estimate for the sdB pulsation frequency, and recognize the presence of an unseen companion. Future work on this object will focus on long-term radial velocity monitoring of this star in order to better constrain the true period of this binary.

8. ACKNOWLEDGMENTS

The authors would like to acknowledge Stéphane Charpinet and JJ Hermes for illuminating discussions. L. N. thanks the Natural Sciences and Engineering Research Council (Canada) for financial support through the Discovery Grants program. G. H. acknowledges support by the Polish NCN grant 2015/18/A/ST9/00578.

This paper includes data collected by the *TESS* mission. Funding for the *TESS* mission is provided by the NASA's Science Mission Directorate. Some computations were carried out on the supercomputers managed by Calcul Québec and Compute Canada. The operation of these supercomputers is funded by the Canada Foundation for Innovation (CFI), and the Fonds de recherche du Québec – Nature et technologies (FRQNT).

This work has made use of data from the European Space Agency (ESA) mission *Gaia* (https://www.cosmos.esa.int/gaia), processed by the *Gaia* Data Processing and Analysis Consortium (DPAC, https://www.cosmos.esa.int/web/gaia/dpac/consortium). Funding for the DPAC has been provided by national institutions, in particular the institutions participating in the Gaia Multilateral Agreement.

We would like to acknowledge the Indigenous Peoples as the traditional stewards of the land on which this research was conducted, and the enduring relationship between them and their traditional territories. We acknowledge the painful history of genocide and forced occupation of their territory, and we honor and respect the many diverse Indigenous people connected to this land on which we research and gather from time immemorial.

Facilities: TESS, Gaia, UKST

Software: SPOC (Jenkins 2015), `numpy` (Harris et al. 2020), `matplotlib` (Hunter 2007), `scipy` (Virtanen et al. 2020), `astropy` (Astropy Collaboration et al. 2013, 2018), `pysynphot` (STScI Development Team 2013), `pandas` (pandas development team 2020; Wes McKinney 2010) , `SPECTRUM` (Gray 1999)

[8] If $M_{1,0} \lesssim 3 M_\odot$, the primary will evolve into a helium white dwarf and never undergo an sdB phase for the range of initial conditions that we considered.

REFERENCES

Andrae, R., Fouesneau, M., Creevey, O., et al. 2018, Astronomy & Astrophysics, 616, A8

Astropy Collaboration, Robitaille, T. P., Tollerud, E. J., et al. 2013, A&A, 558, A33, doi: 10.1051/0004-6361/201322068

Astropy Collaboration, Price-Whelan, A. M., Sipőcz, B. M., et al. 2018, AJ, 156, 123, doi: 10.3847/1538-3881/aabc4f

Belokurov, V., Penoyre, Z., Oh, S., et al. 2020, MNRAS, 496, 1922, doi: 10.1093/mnras/staa1522

Bloecker, T. 1995, A&A, 299, 755

Breger, M., & Bregman, J. N. 1975, ApJ, 200, 343, doi: 10.1086/153794

Brown, A. G. A., Vallenari, A., Prusti, T., et al. 2018, Astronomy & Astrophysics, 616, A1, doi: 10.1051/0004-6361/201833051

Buchhave, L. A., Bakos, G. Á., Hartman, J. D., et al. 2010, ApJ, 720, 1118, doi: 10.1088/0004-637X/720/2/1118

Cardelli, J. A., Clayton, G. C., & Mathis, J. S. 1989, ApJ, 345, 245, doi: 10.1086/167900

Castellani, M., & Castellani, V. 1993, ApJ, 407, 649, doi: 10.1086/172547

Castelli, F., & Kurucz, R. L. 2004, ArXiv Astrophysics e-prints

Cutri, R. M., & et al. 2014, VizieR Online Data Catalog, II/328

Donati, J.-F., Semel, M., Carter, B. D., Rees, D. E., & Collier Cameron, A. 1997, MNRAS, 291, 658, doi: 10.1093/mnras/291.4.658

Dorman, B., & Rood, R. T. 1993, ApJ, 409, 387, doi: 10.1086/172671

Dziembowski, W. A., & Goode, P. R. 1992, ApJ, 394, 670, doi: 10.1086/171621

Eggleton, P. P. 2000, NewAR, 44, 111, doi: 10.1016/S1387-6473(00)00023-3

Eker, Z., Soydugan, F., Soydugan, E., et al. 2015, The Astronomical Journal, 149, 131, doi: 10.1088/0004-6256/149/4/131

Furesz, G. 2008, PhD thesis, University of Szeged

Gaia Collaboration, Prusti, T., de Bruijne, J. H. J., et al. 2016a, A&A, 595, A1, doi: 10.1051/0004-6361/201629272

Gaia Collaboration, Brown, A. G. A., Vallenari, A., et al. 2016b, A&A, 595, A2, doi: 10.1051/0004-6361/201629512

—. 2021, A&A, 649, A1, doi: 10.1051/0004-6361/202039657

Gray, R. O. 1999, SPECTRUM: A stellar spectral synthesis program. http://ascl.net/9910.002

Gray, R. O., & Corbally, C. J. 1994, AJ, 107, 742, doi: 10.1086/116893

Han, Z., Podsiadlowski, P., Maxted, P. F. L., & Marsh, T. R. 2003, MNRAS, 341, 669, doi: 10.1046/j.1365-8711.2003.06451.x

Han, Z., Podsiadlowski, P., Maxted, P. F. L., Marsh, T. R., & Ivanova, N. 2002, MNRAS, 336, 449, doi: 10.1046/j.1365-8711.2002.05752.x

Harris, C. R., Millman, K. J., van der Walt, S. J., et al. 2020, Nature, 585, 357, doi: 10.1038/s41586-020-2649-2

Heber, U. 1986, Spectroscopic Analyses of Hot Extreme Helium Stars (review), ed. K. Hunger, D. Schoenberner, & N. Kameswara Rao, 33, doi: 10.1007/978-94-009-4744-3_4

—. 2016, PASP, 128, 082001, doi: 10.1088/1538-3873/128/966/082001

Holdsworth, D. L., Østensen, R. H., Smalley, B., & Telting, J. H. 2017, MNRAS, 466, 5020, doi: 10.1093/mnras/stx077

Holdsworth, D. L., Saio, H., Sefako, R. R., & Bowman, D. M. 2018, MNRAS, 480, 2405, doi: 10.1093/mnras/sty2039

Hunger, K., & Kudritzki, R. P. 1981, The Messenger, 24, 7

Hunter, J. D. 2007, Computing in Science & Engineering, 9, 90, doi: 10.1109/MCSE.2007.55

Jenkins, J. M. 2015, in AAS/Division for Extreme Solar Systems Abstracts, Vol. 47, AAS/Division for Extreme Solar Systems Abstracts, 106.05

Justham, S., Podsiadlowski, P., & Han, Z. 2011, MNRAS, 410, 984, doi: 10.1111/j.1365-2966.2010.17497.x

Kepler, S. O., Pelisoli, I., Koester, D., et al. 2016, MNRAS, 455, 3413, doi: 10.1093/mnras/stv2526

Kilkenny, D., Koen, C., O'Donoghue, D., & Stobie, R. S. 1997, MNRAS, 285, 640, doi: 10.1093/mnras/285.3.640

Kuiper, G. P. 1941, ApJ, 93, 133, doi: 10.1086/144252

Kurtz, D. W. 1985, MNRAS, 213, 773, doi: 10.1093/mnras/213.4.773

Latour, M., Chayer, P., Green, E. M., Irrgang, A., & Fontaine, G. 2018, A&A, 609, A89, doi: 10.1051/0004-6361/201731496

Lynas-Gray, A. E. 2021, Frontiers in Astronomy and Space Sciences, 8, 19, doi: 10.3389/fspas.2021.576623

Mengel, J. G., Norris, J., & Gross, P. G. 1976, ApJ, 204, 488, doi: 10.1086/154193

Murphy, S. J. 2014, PhD thesis, Jeremiah Horrocks Institute, University of Central Lancashire, Preston, UK

Nelson, L. A., Dubeau, E., & MacCannell, K. A. 2004, ApJ, 616, 1124, doi: 10.1086/421698

Ochsenbein, F., et al. 2019, The VizieR database of astronomical catalogues , doi: 10.26093/cds/vizier

pandas development team, T. 2020, pandas-dev/pandas: Pandas, latest, Zenodo, doi: 10.5281/zenodo.3509134

Paxton, B., Bildsten, L., Dotter, A., et al. 2011, ApJS, 192, 3, doi: 10.1088/0067-0049/192/1/3

Paxton, B., Cantiello, M., Arras, P., et al. 2013, ApJS, 208, 4, doi: 10.1088/0067-0049/208/1/4

Paxton, B., Marchant, P., Schwab, J., et al. 2015, ApJS, 220, 15, doi: 10.1088/0067-0049/220/1/15

Paxton, B., Schwab, J., Bauer, E. B., et al. 2018, ApJS, 234, 34, doi: 10.3847/1538-4365/aaa5a8

Paxton, B., Smolec, R., Schwab, J., et al. 2019, ApJS, 243, 10, doi: 10.3847/1538-4365/ab2241

Prusti, T., de Bruijne, J. H. J., Brown, A. G. A., et al. 2016, Astronomy & Astrophysics, 595, A1, doi: 10.1051/0004-6361/201629272

Reimers, D. 1975, Memoires of the Societe Royale des Sciences de Liege, 8, 369

Ricker, G. R., Winn, J. N., Vanderspek, R., et al. 2015, Journal of Astronomical Telescopes, Instruments, and Systems, 1, 014003, doi: 10.1117/1.JATIS.1.1.014003

Ritter, A. 1879, Annalen der Physik, 244, 157, doi: 10.1002/andp.18792440910

Saffer, R. A., Bergeron, P., Koester, D., & Liebert, J. 1994, ApJ, 432, 351, doi: 10.1086/174573

Schindler, J.-T., Green, E. M., & Arnett, W. D. 2015, ApJ, 806, 178, doi: 10.1088/0004-637X/806/2/178

Senhadji, A. 2019, Master's thesis, Bishop's University. https://www.abdelbassitsenhadji.com/masters-thesis

Skrutskie, M. F., Cutri, R. M., Stiening, R., et al. 2006, AJ, 131, 1163, doi: 10.1086/498708

Smith, M. A. 1973, ApJS, 25, 277, doi: 10.1086/190270

Stassun, K. G., Oelkers, R. J., Paegert, M., et al. 2019, AJ, 158, 138, doi: 10.3847/1538-3881/ab3467

Stellingwerf, R. F. 1979, ApJ, 227, 935, doi: 10.1086/156802

STScI Development Team. 2013, pysynphot: Synthetic photometry software package. http://ascl.net/1303.023

Tauris, T. M., & van den Heuvel, E. P. J. 2006, Formation and evolution of compact stellar X-ray sources, Vol. 39, 623–665

Virtanen, P., Gommers, R., Oliphant, T. E., et al. 2020, Nature Methods, 17, 261, doi: 10.1038/s41592-019-0686-2

Vos, J., Vučković, M., Chen, X., et al. 2019, Contributions of the Astronomical Observatory Skalnate Pleso, 49, 264

Webbink, R. F. 1976, ApJ, 209, 829, doi: 10.1086/154781

Werner, K., Dreizler, S., & Rauch, T. 2012, TMAP: Tübingen NLTE Model-Atmosphere Package. http://ascl.net/1212.015

Wes McKinney. 2010, in Proceedings of the 9th Python in Science Conference, ed. Stéfan van der Walt & Jarrod Millman, 56 – 61, doi: 10.25080/Majora-92bf1922-00a

Winget, D. E. 1998, Journal of Physics: Condensed Matter, 10, 11247, doi: 10.1088/0953-8984/10/49/014

Winget, D. E., & Kepler, S. O. 2008, ARA&A, 46, 157, doi: 10.1146/annurev.astro.46.060407.145250

Xiong, H., Chen, X., Podsiadlowski, P., Li, Y., & Han, Z. 2017, A&A, 599, A54, doi: 10.1051/0004-6361/201629622

Zhou, G., Rappaport, S., Nelson, L., et al. 2018, ApJ, 854, 109, doi: 10.3847/1538-4357/aaa9b9